Image Anal Stereol 2024;43:67-84 doi: 105566/ias.3009
Original Research Paper

IMPROVING THE MACHINE LEARNING PERFORMANCE FOR IMAGE RECOGNITION USING A NEW SET OF MOUNTAIN FOURIER MOMENTS

YAHYA SAHMOUDI✉,[1], OMAR EL OGRI[1,2], JAOUAD EL-MEKKAOUI[1], BOUJAMAA JANATI IDRISSI[1], AMAL HJOUJI[2]

[1]LTI, Laboratory, EST, Sidi Mohamed Ben Abdellah University, Fez, Morocco; [2]CED-ST, STIC, Laboratory of Information, Signals, Automation and Cognitivism LISAC, Dhar El Mahrez Faculty of Science, Sidi Mohamed Ben Abdellah-Fez University, Fez, Morocco
e-mail: yahya.sahmoudi@usmba.ac.ma, omar.elogri@usmba.ac.ma, jawad.mekkaou@gmail.com, boujamaa.janatiidrissi@usmba.ac.ma, hjouji.amal@gmail.com
(Received August 19, 2023; revised February 17, 2024; accepted February 17, 2024)

ABSTRACT

The orthogonal moments are giving relevant results of these last years within the framework of object detection, pattern recognition and image reconstruction. This article is based on orthogonal functions called "Orthogonal Mountain functions (OMFs)" and we introduce a new set of moments called the multichannel Mountain Fourier moments (MMFMs), their performance is in reconstruction, noise invariants, rotation, scale and translation for image color. To validate these proposed techniques, we made several experimental tests to analyse images. We compare the results obtained from invariant moments and other current orthogonal invariant moments; the experiments show the power of the proposed moments.

Keywords: K-nearest neighbours (KNN), Mountain Fourier invariant moments, Multichannel invariant moments, orthogonal Mountain functions, pattern recognition, support vector machine (SVM).

INTRODUCTION

For image recognition and representation images, one applies one of the techniques which transform an image into a vector by requiring a decision to be made based on the specific class to that image. Clearly, the extracted feature vector is what gives the quality of the image representation. For this characteristic to be powerful, it must be at least invariant in rotation, in translation and in scale. And for this reason, in recent years, applications on image analysis and pattern recognition have known very important developments including; image identification by Hu (1962), collected and image recovery by Teague (1980), infrared analysis by Zhang *et al.* (2009), English and Chinese Letters analysis by Hjouji *et al.* (2021a), walking detection by Lahouli *et al.* (2018), dot spots by Hjouji *et al.* (2021b), image noise by Ji *et al.* (2009), face identification by El-Mekkaoui *et al.* (2021), image description by Hosny and Darwish (2018), color form test by Assefa *et al.* (2010), 3Dim image identification by Batioua *et al.* (2017), image content by Singh (2012), image evaluation by El Ogri *et al.* (2020), robust detection by Chen *et al.* (2018), pattern storage by Hmimid *et al.* (2015), use of sketches by Ansary *et al.* (2006), scene report by Lin *et al.* (2008), eye diseases detection and classification by Jenny *et al.* (2023), correction of noisy images by Chen *et al.* (2022), an accurate segmentation of the object of interest by Vite-Chávez *et al.* (2023) …etc. In this article we base ourselves on the principles of orthogonal moments, Hu (1962) first proposed an extraction feature using non-orthogonal invariant moments. After a few years, the idea of orthogonal moments was introduced by Teague (1980) which is based on orthogonal polynomials; we find Zernike, Laguerre, Jacobi and Legendre. We used a circular scale of polar coordinates on a disc of radius 1 to define the proposed moments, like moments of Zernike by Kim *et al.* (2000) and Kanaya *et al.* (2002), moments of Legendre by Xiao *et al.* (2014), moments of pseudo Zernike by Bailey *et al.* (1996), moments of Fourier Chebyshev by Ping *et al.* (2002), moments of Fourier Mellin by Sheng *et al.* (1994), Radian-harmonic by Ren *et al.* (2003), moments of Fourier Bessel by Xiao *et al.* (2010), Harmonic polar by Yap *et al.* (2009), Fourier exponent by Hu *et al.* (2014) and Fourier Harmonic polar by Wang *et al.* (2019). As these moments are invariant in rotation, we conclude that we have a very important characteristic in image

recognition. One can use the same principle to express on the basis of the polar coordinates and the descriptor matrices of the color images in invariant multichannel orthogonal moments, such as the moments of Fourier harmonics by Wang *et al.* (2018), the moments of Zernike quaternions (QZM) by Chen *et al.* (2012), multichannel orthogonal radial Chebyshev (MRSCMs) by Hosny *et al.* (2019), multichannel orthogonal Zernike (MZMs) by Singh *et al.* (2018), quaternion Pseudo Zernike (QPZMs) by Bao *et al.* (2019), quaternion Fourier Mellin (QFMMs) by Guo *et al.* (2011), generalized orthogonal quaternions Fourier Chebyshev (QGCFMs) and pseudo Jacobi Fourier (QPJFMs) Singh *et al.* (2018). If the distance between the moment of a normal image and the moment of the same image which has been geometrically transformed tends to be 0, then the moment is reliable and solid, and these moments represent the image descriptor vector which are real or complex values. To extract the invariants of the proposed moments, we used the principle of the theoretical method of numerical approximations which makes it possible to transform the integral to the addition because the moments are defined on integrals based on orthogonal functions called Mountain functions.

We have proposed new moments, called multi-channel orthogonal Fourier Mountain moments (MMFMs). We must have in the progress of this article; that the model is more efficient and invariant in rotation, in translation and in scale, moreover, the calculated average CPU times of proposed moments (MMFMs) should be very fast compared to the tested invariant moments. The main contribution of the proposed methods are as follows:

- Presentation of the proposed orthogonal Mountain functions (OMFs).
- Introduction of a new set of multichannel orthogonal Fourier-Mountain moments (MMFMs) based on orthogonal mountain functions (OMFs).
- Test of the capacity of proposed moments MMFMs regarding the reconstruction of images either for geometric transformations; the rotation, the scale and the translation or for noisy images.
- Comparison of the results obtained with different well-known orthogonal moments in terms of reconstruction and classification.
- We have to use for classification two techniques; the first is MMFMs-KNN architecture using K-NN, and the second is MMFMs-SVM architecture using SVM classifier.
- We calculate the average CPU times of the proposed moments (MMFMs) and compare them with the invariant moments of the test.

The axis of this article are organized as follows; in the section 2, presentation the orthogonal Mountain functions (OMFs). The proposed moments: multichannel orthogonal Fourier Mountain moments (MMFMs) and their geometric invariants for color images and all aspects are introduced in Sections 3. Section 4 presents the adopted computational methods and proposed overall system. The experimental and discussion are presented in section 5 and 6. Finally in section 7 we give a conclusion of this work.

RELATED WORKS

Several works for image reconstruction and classification based on two-dimensional orthogonal moments and moment invariants have been presented in the literature. In recent years, an increasing number of researchers have shown real interest in the study of images moments. Fractional quaternion Zernike moments for robust color image copy-move forgery detection by Chen *et al.* (2018), new set of multichannel orthogonal moments for color image representation and recognition by Hosny *et al.* (2019), image classification using shifted Legendre Fourier moments and deep learning by Machhour *et al.* (2019), fractional quaternion cosine transform and its application in color image copy-move forgery detection by Yu *et al.* (2019), new fractional order Legendre Fourier moments for pattern recognition applications by Hosny *et al.* (2020), novel fractional order polar harmonic transforms for gray-scale and color image analysis by Darwish *et al.* (2020), image recognition using new set of separable three dimensional discrete orthogonal moment invariants by Batioua *et al.* (2020), a new separable moments based on Chebyshev Krawtchouk polynomials by Idan *et al.* (2020), accurate 2D and 3D images classification using translation and scale invariants of Meixner moments by Yamni *et al.* (2021), new fractional order shifted Gegenbauer moments for image analysis and recognition by Aboelenen *et al.* (2020), a survey of orthogonal moments for Image representation: theory, implementation, and evaluation by Qi *et al.* (2021), a robust handwritten numeral recognition using hybrid orthogonal polynomials and moments by Abdulhussain *et al.* (2021),quaternion fractional order color orthogonal moment based image representation and recognition by He *et al.* (2021), 3D image recognition using new set of fractional order Legendre moments and deep neural networks by El Ogri *et al.* (2021), face recognition algorithm based on fast computation of

orthogonal moments by Abdulhussain *et al.* (2022), an efficient computation of discrete orthogonal moments for bio-signals reconstruction by Fathi *et al.* (2022), a new retrieval system based on quaternion radial orthogonal Jacobi moments for biomedical color images by Janati Idrissi *et al.* (2024). The modulus of these moments' invariants is a crucial property in image recognition. This kind of orthogonal moments tends to express and recognize images. Similarly, using polar coordinates, the descriptor vectors for color images can be revealed via multichannel orthogonal. The quality and applicability in the field of pattern recognition are necessarily affected by the use of numerical approximations during the process of computing and extracting the invariants from these moments.

ORTHOGONAL MOUNTAIN FUNCTIONS

This part is divided into three axis; the first presents the new set of Mountain functions (OMFs) similar with the strictly increasing sequence of regular steps $\{r_i, \mathrm{i} = 1, \dots, \mathrm{N}\}$. The second shows the property of discrete orthogonality. In the third we use the polar coordinates to define all orthogonal Mountain functions.

The Mountain functions

These functions are defined from two main properties:

Property 1. A finite strictly increasing sequence of regular step d is a finite succession $\{r_i, i = 1, \dots, N\}$ of real numbers such that

$$r_1 < r_2 < \cdots < r_N \ \ and \ \ |r_{i+1} - r_i| = d\,, \quad for\ all\ i = 1, \dots, N; \tag{1}$$

Property 2. The collection of Mountain functions $\{M_j, j = 1, \dots, N\}$ with the strictly increasing sequence of regular steps $\{r_i, \mathrm{i} = 1, \dots, \mathrm{N}\}$ is defined as

$$M_j(x) = \begin{cases} 1 - \left(\frac{x - r_j}{d}\right)^2 & if\ x \in [r_j - d, r_j + d] \\ 0 & elsewhere \end{cases} \tag{2}$$

Fig.1 presents the Mountain functions (OMFs) associated with the strictly increasing sequence of regular steps $\{1,2,\dots,6\}, \{1,2,\dots,12\}$, $\{1,2,\dots,25\}$ and $\{1,2,\dots,50\}$.

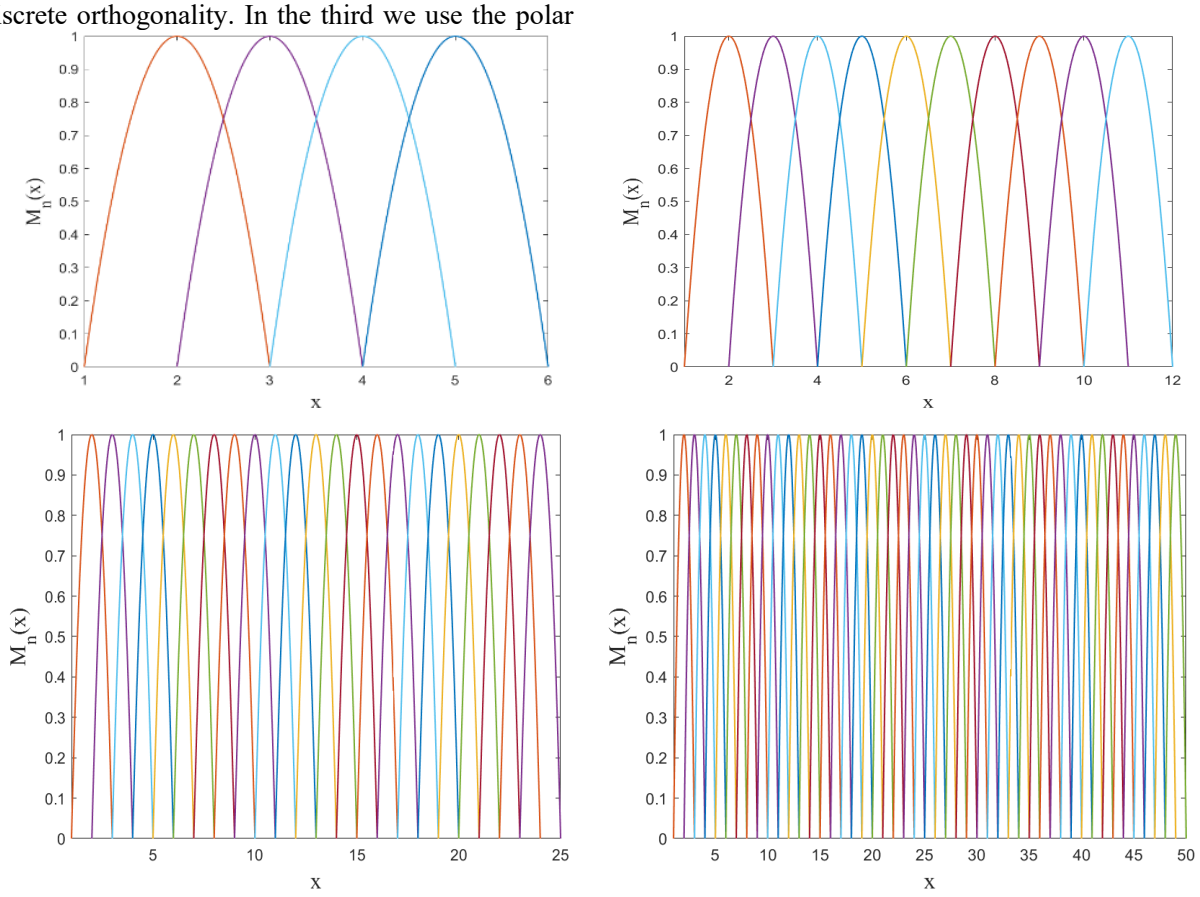

Fig. 1. *Graph of orthogonal mountain functions (OMFs) associated with the strictly increasing sequence of regular steps (a)* $\{1,2,\dots,6\}$*, (b)* $\{1,2,\dots,12\}$*, (c)* $\{1,2,\dots,25\}$ *and (d)* $\{1,2,\dots,50\}$.

Discrete orthogonality of Mountain functions

Note first that the Mountain functions presented in Eq.2 satisfy the following lemma.

Lemma:

$$\begin{cases} M_n(r_n) = 1, \ for\ all\ n = 1,.. \\ M_n(r_j) = 0, \ \ for\ all\ j \neq n \end{cases} \quad (3)$$

Based on equation (3), we can see that:

If $m \neq n$ we have $M_n(r_i)M_m(r_i) = 0$ for all i = 1, … , N, then

$$\sum_{j=1}^{N} M_n(r_j)M_m(r_j) = 0 \quad (4)$$

else

$$\sum_{i=1}^{N} M_k(r_i)M_k(r_i) = M_k(r_k)M_k(r_k) = 1 \quad (5)$$

Therefore, the discrete orthogonality condition Eq.6 holds for the set of Mountain functions:

$$\sum_{i=1}^{N} M_n(r_i)M_m(r_i) = \delta_{nm} \quad (6)$$

Orthogonal Mountain Fourier functions coupled to color image

Hosny *et al.* (2011) modified the technique presented by Xin *et al.* (2007) which allows to map the color image from rectangle to circle, as shown in Fig.2. We take an image of size 2N × 2N and we obtain a new arrangement diagram of pixels. The unit disk Fig.2 is divided into N rings along the radial direction

$$\{r_k = k, k = 1, \dots, N\} \quad (7)$$

In Fig.2, we separate the RGB color then transform into polar coordinates so that the number of rings "i" can be divided into 4+8i equal parts determined by the angles α_{ik} then we combine the three colors.

$$\alpha_{ik} = \frac{2\pi(k+0.5)}{4+8i}, k = 0, \dots, 3 + 8i \quad (8)$$

We consider the strictly increasing sequence of regular steps $\{r_k = k, k = 1, \dots, N\}$. The step of this strictly increasing sequence is $Step = 1$. The set of mountain functions $\{M_1, M_2, \dots, M_{\mathrm{N}},\}$ associated with the sequence $\{r_k = k, k = 1, \dots, N\}$ is defined as

$$M_n(x) = \begin{cases} 1 - (x - n)^2 \ \ if\ x \in [\mathrm{n} - 1, \mathrm{n} + 1] \\ 0 \quad\quad elsewhere \end{cases} \quad (9)$$

Then, our basis function is the set

$$D_{lz}(r_j, \alpha_{jk}) = M_l(r_j)e^{im\alpha_{jk}}, \quad for\ l = 1,..,N\ and\ z \in \mathbb{Z} \quad (10)$$

Where $i^2 = -1$ and $e^{im\alpha_{jk}}$ is the complex polynomials. These polynomials are also orthogonal, the orthogonality demonstration is presented in Appendix 1.

Moreover,

$$\sum_{k=0}^{3+8j} e^{in\alpha_{jk}} e^{im\alpha_{jk}} = \sum_{k=0}^{3+8j} e^{i\frac{2\pi n(k+0.5)}{4+8j}} e^{-i\frac{2\pi m(k+0.5)}{4+8j}} = (4 + 8j)\delta_{nm} \quad (11)$$

The orthogonality of $D_{lz}(r_j, \alpha_{jk})$ demonstration is presented in Appendix 2.

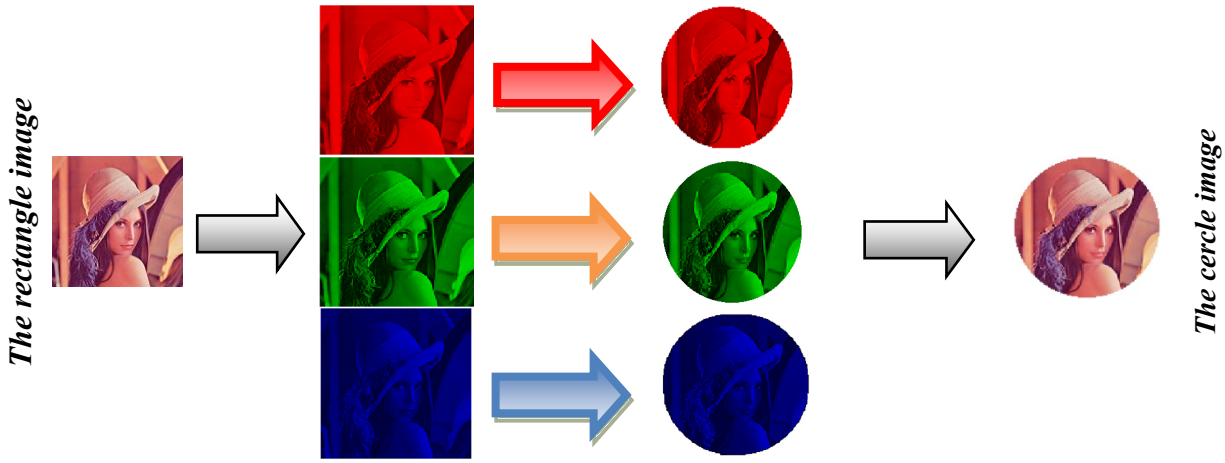

Fig. 2. *The image RGB mapped from rectangle to cercle image.*

THE PROPOSED MOMENTS AND INVARIANCE TO THE GEOMETRIC TRANSFORMATIONS

We have divided this section into two parts; the first subsection presents the proposed moments (MMFMs). The second subsection verifies the invariants of MMFMs for rotation, translation and scale.

The proposed moments multichannel orthogonal mountain Fourier moments

Each color image $f(r,\alpha)$ is represented by three primary channels Red(R), Green(G) and Blue(B), i.e

$$f(r,\alpha) = \left(f_R(r,\alpha), f_G(r,\alpha), f_B(r,\alpha)\right) \quad (12)$$

In order $(n+m)$, the proposed moments MMFMs for the image $f(r,\alpha)$ are defined as:

$$MMF_{nm}(f) = \left(MMF_{nm}(f_R), MMF_{nm}(f_G), MMF_{nm}(f_B)\right) \quad (13)$$

where $MMF_{nm}(f_Q), Q \in \{R,G,B\}$ is defined by:

$$MMF_{nm}(f_Q) = \sum_{j=1}^{N}\sum_{k=0}^{3+8j} \frac{1}{4+8n} M_n(r_j) e^{-im\alpha_{jk}} f_P(r_j,\alpha_{jk}) \quad (14)$$

With Eq.3 gives:

$$MMF_{nm}(f_Q) = \sum_{k=0}^{3+8n} \frac{1}{4+8n} e^{-im\alpha_{nk}} f_Q(r_n,\alpha_{nk}), \quad (15)$$
$$for\ all\ n = 1,\dots,N\ and\ m \in \mathbb{Z}$$

For $Q \in \{R,G,B\}$, we take a finite number of MMFMs to approximately reconstruct the color image $f(r,\alpha)$ as follows:

$$\hat{f}_Q(r_j,\alpha_{jk}) = \sum_{n=1}^{Max}\sum_{m=-mMax}^{mMax} MMF_{nm}(f)\, M_n(r_j) e^{im\alpha_{jk}} \quad (16)$$

The invariance to geometric transformations of MMFMs

We have to present a new mathematical formula in these following parts which shows the rotation, translation and scaling invariances of the proposed moments because these geometric transformations play roles of power and performance of each moment.

Rotation invariance of MMFM

We will conclude from Wang X. Y. *et al.* (2015) that the calculated moments MMFMs of the color image are invariant to rotation.

Let $f^{\alpha_0}(r,\alpha)$ rotated image $f(r,\alpha)$of the original image $f(r,\alpha) = \left(f_R(r,\alpha), f_G(r,\alpha), f_B(r,\alpha)\right)$. The image treated is color image for that one must study the invariance of rotation of the three levels of gray, to obtain $MMF_{nm}(f_Q^{\alpha_0})$ of $f^{\alpha_0}(r,\alpha)$, as a function of $MMF_{nm}(f_Q)\ of\ f_Q(r,\alpha)$, as follows ,as follows

$$MMF_{nm}(f_Q^{\alpha_0}) = e^{im\alpha_0} MMF_{nm}(f_Q), \quad \forall Q \in \{R,G,B\} \quad (17)$$

Therefore,

$$\left|MMF_{nm}(f_Q^{\alpha_0})\right| = \left|MMF_{nm}(f_Q)\right|, \quad \forall Q \in \{R,G,B\} \quad (18)$$

Then we can follow the same technique to re-formulate NMMFMs of proposed moments MMFMs to show invariants to rotation, as follows:

$$NMMF_{n,l}(f_Q) = MMF_{n,,m}(f_Q).MMF_{l,-m}(f_P), \forall Q \in \{R,G,B\} \quad (19)$$

Translation invariance of MMFMs

We follow the same technique of Suk T. *et al.* (2009) for translation invariance by moving the origin of the coordinates to the barycentre $(\bar{x},\bar{y})$ of the color image f, such that

$$\bar{x} = \frac{m_{10}(f_R) + m_{10}(f_G) + m_{10}(f_B)}{m_{00}} \quad (20)$$

$$\bar{y} = \frac{m_{01}(f_R) + m_{01}(f_G) + m_{01}(f_B)}{m_{00}} \quad (21)$$

$$m_{00} = m_{00}(f_R) + m_{00}(f_G) + m_{00}(f_B) \quad (22)$$

Such that each f_Q color channel is associated with these calculated moments $m_{pq}(f_Q); p,q = 0;1;2....$

Scale invariance of MMFMs

Let $f^s(r,\alpha)$ is the scale version image of the original image $f(r,\alpha)$) with $f(r,\alpha) = \left(f_R(r,\alpha), f_G(r,\alpha), f_B(r,\alpha)\right)$ with factor s of the $f(r,\alpha)$The image treated is a color image. For that, one must study the invariance of scale of the three gray-levels images. To obtain $MMF_{nm}(f_Q^s)$ of $f^s(r,\alpha)$, as follow

$$MMF_{nm}(f_Q^s) = \frac{1}{N_n}\sum_{t=0}^{N_n-1} e^{-i.\overline{\alpha_{nk}}}.f_Q\left(\frac{\overline{r_n}}{s}, \overline{\alpha_{nt}}\right) \quad (23)$$

by the changing $\overline{r'_n} = \frac{\overline{r_n}}{s}$, we have

$$MMF_{nm}(f_Q^s) = \frac{1}{N_n}\sum_{t=0}^{N_n-1} e^{-i.\overline{\alpha_{nk}}}.f_X(\overline{r'_n}, \overline{\alpha_{nt}}) = MMF_{nm}(f_Q), Q = \{R,G,B\} \quad (24)$$

COMPUTATIONAL TECHNIQUES AND PROPOSED OVERALL SYSTEM

The adopted computational methods

We must adopt the cartesian image pixels to the polar image pixels technique which is developed by Xin Y. *et al.* (2007) and improved by Hosny K. M. *et al.* (2011) to calculation of the proposed moments MMFMs on images of size $2N \times 2N$ with concentric circles. We use the radial direction to divide the disk into N rings, we limit each ring by two circles of rays $\left\{r_k == \frac{k}{N} \text{ and } r_{k+1} = \frac{k+1}{N};\ k = 0,1,2\ldots,N-1\right\}$, and each number i of ring contains numbers 4+8j equals parts determined by the angles α_{ix}. As illustrated in Fig.4.

$$\alpha_{ix} = \frac{2(x+\frac{1}{2})\pi}{4+8i}, x = 0,\ldots,4+8i. \quad (25)$$

Then we calculate for the discrete image the moments (MFMs) presented in Eq.15 by a numerical integral $\{f(r_i,\alpha_{ix}),\ i = 0,1,2\ldots,N-1,\ x = 0,\ldots,4+8i\}$ of size $N \times 2N$ as follows:

$$MF_{nm}(f) = \frac{1}{2\pi}\int_0^1\int_0^{2\pi} f(r,\alpha)M_n(r)e^{-jm\alpha}\,r\,dr\,d\alpha \approx \frac{1}{2\pi}\sum_{i=1}^{N}\sum_{x=0}^{3+8i} M_n(r_i)r_i e^{-jm\alpha_{jk}} f(r_i,\alpha_{ix})\,\nabla r_j \nabla\alpha_{jx} \quad (26)$$

where

$$\nabla r_i = r_{i+1} - r_i = \frac{i+1}{N} - \frac{i}{N} = \frac{1}{N}) \quad (27)$$

$$\nabla\alpha_{ix} = \alpha_{i,x+1} - \alpha_{i,x} = \frac{2\pi(x+1+0.5)}{4+8i} - \frac{2\pi(x+0.5)}{4+8i} = \frac{2\pi}{4+8i} \quad (28)$$

with

$$\begin{cases} M_n(r_n) = \dfrac{d}{\sqrt{r_n}} = \dfrac{\frac{1}{2N}}{\sqrt{\frac{n}{N}}} = \dfrac{1}{2\sqrt{nN}} & for\ all\ n = 1,.. \\ M_n(r_j) = 0, & for\ all\ j \neq n \end{cases} \quad (29)$$

We use Eq.29 in Eq.26, we get

$$MF_{nm}(f) \approx \frac{1}{2\pi}\sum_{x=0}^{3+8i} M_n(r_n)r_n e^{-jm\alpha_{nx}} f(r_n,\alpha_{nx})\nabla r_n \nabla\alpha_{nx}$$

$$MF_{nm}(f) \approx \frac{r_n\nabla r_n}{4\pi\sqrt{nN}}\sum_{x=0}^{3+8n} e^{-jm\alpha_{nx}} f(r_n,\alpha_{nx})\nabla\alpha_{nx} \quad (30)$$

by substituting Eq.27, Eq.28 and $r_n = \frac{n}{N}$ in Eq.30, we get

$$MF_{nm}(f) \approx \frac{\sqrt{n}}{2N^2\sqrt{N}(4+8n)}\sum_{x=0}^{3+8n} e^{-jm\alpha_{nx}} f(r_n,\alpha_{nx}) \quad (31)$$

Also, the calculation of the moments MMFMs present in Eq.15 as following:

$$MMF_{nm}(f_Q) \approx \frac{\sqrt{n}}{2N^2\sqrt{N}(4+8n)}\sum_{x=0}^{3+8n} e^{-jm\alpha_{nx}} f_Q(r_n,\alpha_{nx}), \quad Q \in \{R,G,B\} \quad (32)$$

From Eq.16, we have the color image reconstruction formula:

$$\hat{f}_Q(r_i,\alpha_{ix}) = \sum_{n=0}^{nMax}\sum_{m=-mMax}^{mMax} MMF_{nm}(f_Q)M_n(r_i)e^{jm\alpha_{ix}} \quad (33)$$

For all $i = 0,1,2\ldots,N-1,\ x = 0,\ldots,4+8i$

From Eq.29 and Eq.33 we deduce

$$\begin{cases} \hat{f}_Q(r_i,\alpha_{ix}) = \dfrac{1}{2\sqrt{iN}}\sum_{m=-mMax}^{mMax} MMF_{im}(f_Q)\,e^{jm\alpha_{ix}} & if\ i \le Max \\ \hat{f}_Q(r_i,\alpha_{ix}) = 0 & if\ i > Max \end{cases} \quad (34)$$

Proposed model for object recognition by MMFMsadopted computational methods

We use in this article for image recognition an application of MMFMs using machine learning SVM and KNN. After pre-processing, we obtain a characteristic vector which allows to do the learning. The proposed method is illustrated in Fig.3. To do the test, we take a test image, we calculate the MMFMs moments to obtain the final characteristic vector for the test image, so to get the decision about the target value we compare with the data space of the SVM decision limit.

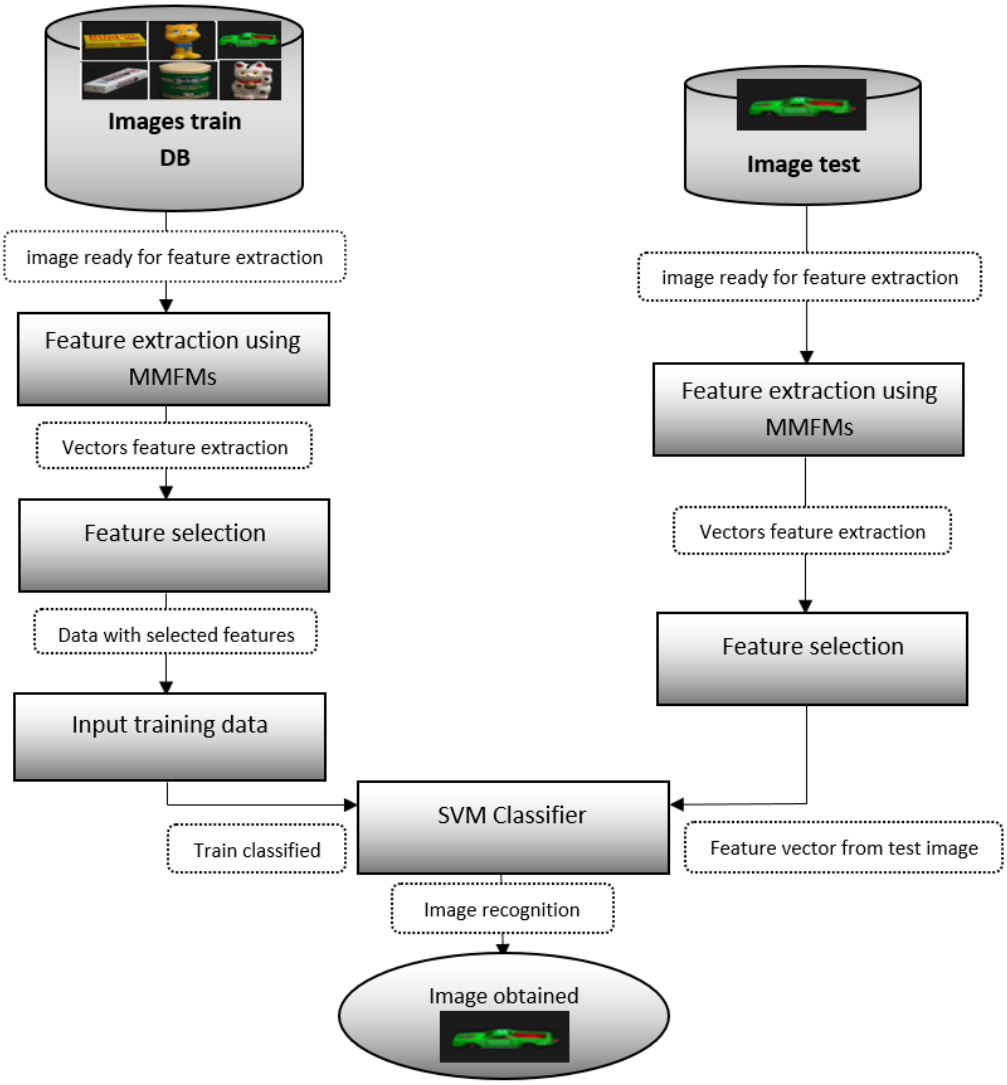

Fig.3: *Block diagram for images recognition.*

EXPERIMENTS RESULTS

We explain in these three upcoming parts; the powers of the moments proposed and the techniques used. In the first, we evaluate the power of MMFMs for image reconstruction. In the second, we present the experiments carried out which make it possible to clarify the invariance of the orthogonal moments proposed MMFMs with respect to translation, rotation and scaling transformations and to noise. In the last part, we must present the precisions of the proposed descriptor vector for classification and recognition. In this work, we used four image databases; COIL_100 Nene *et al.* (1996), ETHZ_53Obj VIS @ ETH Zurich (2003), Caltech_101 Li *et al.* (2022) and 256_ObjectCategories Griffin (2007) to study image situations according to geometric transformations, noise and normal image, and we compare with some invariant moments; multichannel Chebyshev substituted radial invariant (MRSCMs) Hosny *et al.* (2019), multichannel Zernike (MZMs) Singh *et al.* (2018), fractional order multichannel Fourier-Jacobi (FrMJFMs) Aboelenen *et al.* (2020), fractional order Fourier-Legendre (MFrLFMs) Hosny *et al.* (2020) and multichannel fractional order radial Fourier-harmonic (FrMRHFMs) Darwish *et al.* (2020). After all, the efficiency of the proposed moments is related to CPU response time. By comparing the precisions that we found during learning to show the excellence of our proposed method compared to existing methods MRSCMs, MZMs, FrMJFMs, MFrLFMs and FrMRHFMs. Experiments and algorithms are implemented and executed using a following system; Processor (Intel(R)Core (TM) i5-4200M CPU @ 2, 5 GHz), Memory (8GB) and Microsoft Windows 64 bits under MATLAB R2019b.

Algorithm:

Reconstruction image color using multichannel orthogonal Mountain Fourier Moment

Inputs:	
n: The maximum order of moments and f:	
The origin image color.	
Output:	
The color image reconstructed $\hat{f}$	
Step 1	*Compute Mountain functions $M_n(x)$ sing Eq. (9).*
Step 2	*Compute multichannel orthogonal Mountain Fourier moments $MMF_{nm}(f_Q)$ using Eq.32*
Step 3	*Compute image reconstructed $\hat{f}_Q$ for each color Q= {R, G, B} using Eq.34*
Step 4	*We obtain the color image reconstructed $\hat{f}$ by the concatenation of $\hat{f}_Q$ with Q= {R, G, B}*

Image Reconstruction by MMFMs

We employed the color images and the proposed MMFMs moments to reconstruct it using the Eq.34, algorithm shows the different steps of image reconstruction and using Eq.35 which represents the NIRE error to analyse the reconstruction.

$$NIRE = \frac{\sum_{x=0}^{N-1}\sum_{y=0}^{M-1}(f(x,y)-f^{re}(x,y))^2}{\sum_{x=0}^{N-1}\sum_{y=0}^{M-1}(f(x,y))^2} \quad (35)$$

According to the results that we have found and which are presented in Fig.4, we can conclude that our proposed moments MMFMs for the reconstruction of the images are similar to the original image when the max order arrives at 63.

The visualization could easily give the quality of the simulation between the original image and the reconstructed image. Fig.5 gives experimental studies of the NIRE error with respect to some existing invariant moments MRSCMs, MZMs, FrMJFMs, MFrLFMs and FrMRHFMs.

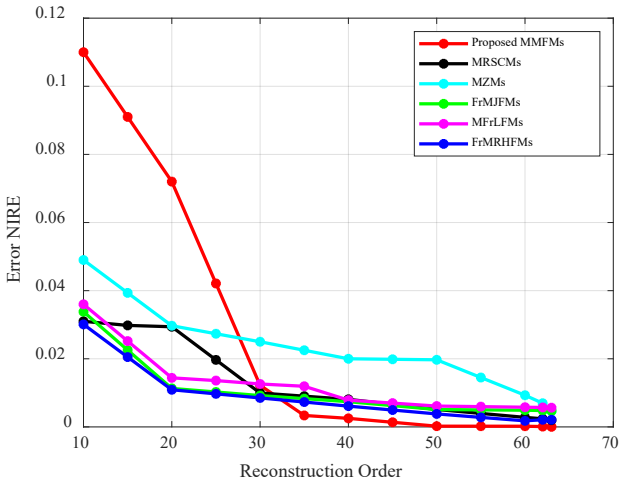

Fig.5. *The variation of reconstruction NIRE error according to the maximum order.*

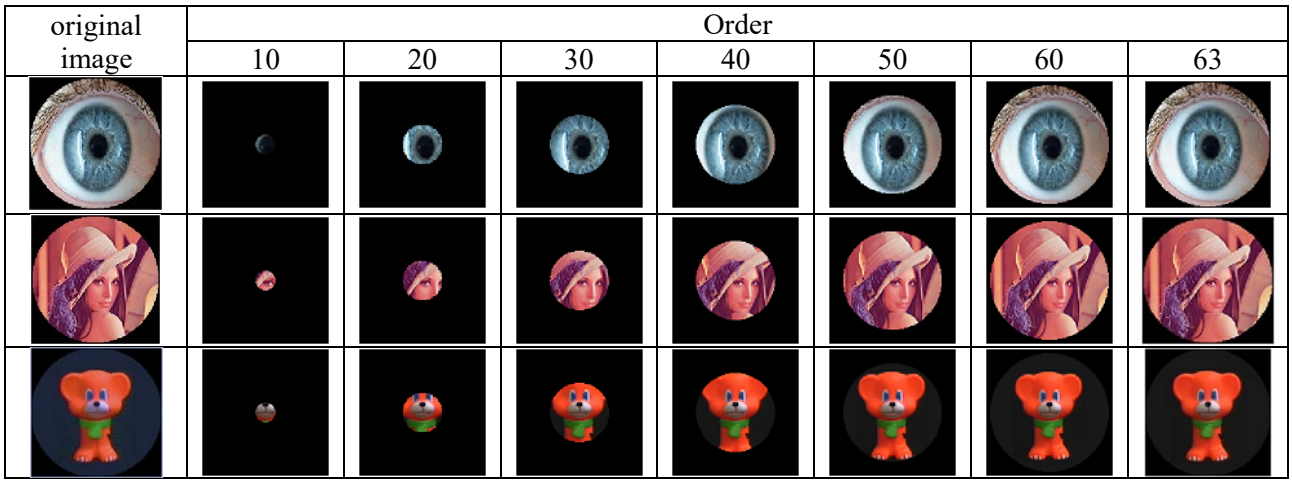

Fig.4. *Reconstructed color images ' 128×128 ' using the proposed moments (MMFMs).*

The geometric transformations and noise in the image

The study of geometric and noisy transformations is essential in this work to know the object exactly in the image.

We worked on the color images Fig.6 to assess the stability quality of the proposed moments MMFMs to remain invariant under different image transformations and noise. We use the relative error (RE) between moments of the original image $M(f)$ and moments of the transformed image $M(f^{tr})$, which is defined as follows:

$$RE(f, f^{tr}) = \frac{\|M(f) - M(f^{tr})\|}{\|M(f)\|} \quad (36)$$

$M(f)$, $M(f^{tr})$ and $\| \|$ respectively, designate moments of the original image f, moments of the transformed image f^{tr} and the Euclidean norm.

$$||M(f)|| = \sqrt{||M(f_R)||^2 + ||M(f_G)||^2 + ||M(f_B)||^2} \quad (37)$$

The good result which has a very low or negligible relative error.

The geometric transformations using MMFMs

In this experiment, we have to verify the invariants derived from the MMFMs must be identical with error tending to 0 if the image is transformed. For this we use the color image Fig.6 of size 128×128. Figs. 8, 10 and 12 to show some transformed images.

We also compared the error results of the proposed

Fig.6. *The color images (a), (b) and (c).*

MMFMs moments and some recent orthogonal invariant moments; MRSCMs, FrMJFMs, MFrLFMs and FrMRHFMs. Figs. 8,10 and 12, we present the results obtained from the RE error for the study carried out. According to the obtained results, we can say that proposed moments MMFMs are more powerful. Then these moments could be effective techniques for image recognition.

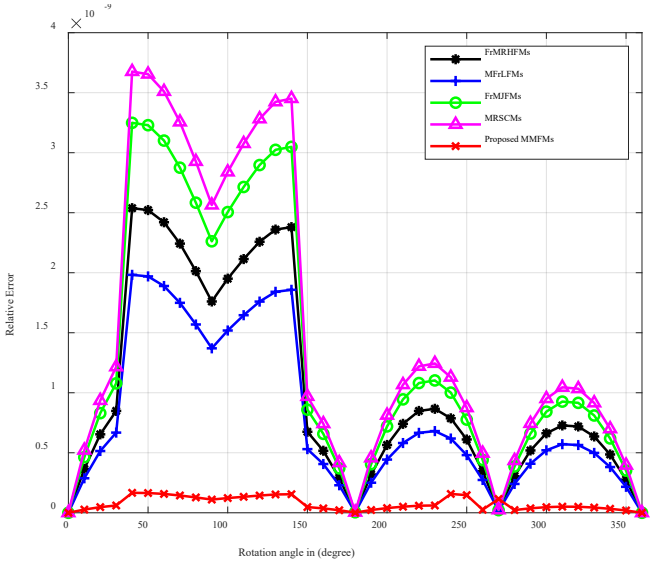

Fig.8. *RE error for the rotated images.*

$r = 0°$ $r = 30°$ $r = 60°$ $r = 90°$ $r = 120°$ $r = 150°$ $r = 180°$

Fig.7: *Rotated images.*

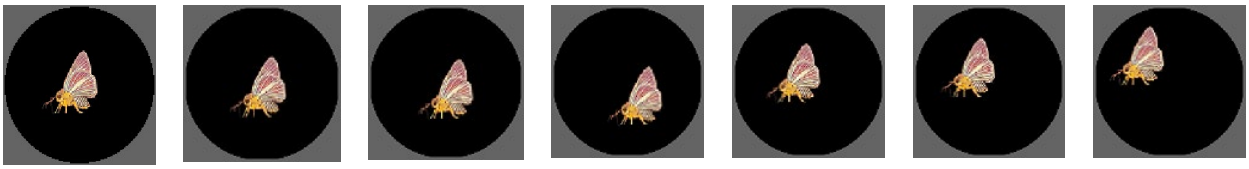

$\vec{v}(0;0)$ $\vec{v}(5;5)$ $\vec{v}(8;8)$ $\vec{v}(15;15)$ $\vec{v}(-5;-5)$ $\vec{v}(-10;-10)$ $\vec{v}(-20;-20)$

Fig.9. *Translated images.*

First experiment: The color image of Fig.6 (a) with size 128 × 128 is rotated by different angles from 0° to 90° in the counter-clockwise direction Fig.7. We have evaluated the RE error for the rotated images, using the proposed moments MMFMs and the other test moments, the results obtained are displayed in Fig.8.

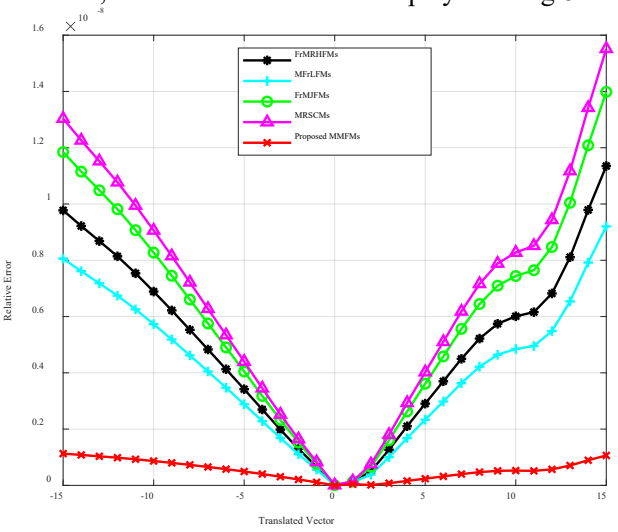

Fig.10. *RE error for the translated images*

Second experiment: The color image of Fig.6(b) with size 128 × 128 is translated using various translation parameters in horizontal and vertical directions Fig.9. We have evaluated the RE error for the translated images, using the proposed moments MMFMs and the other test moments, the results obtained are displayed in Fig.10.

Third experiment: The color image of "Fig.6(c)" with size 128 × 128 is scaled using seven reduction scaling factors Fig.11. We have evaluated the RE error for the scaled images using the proposed moments MMFMs and the other test moments, the results obtained are displayed in Fig.12

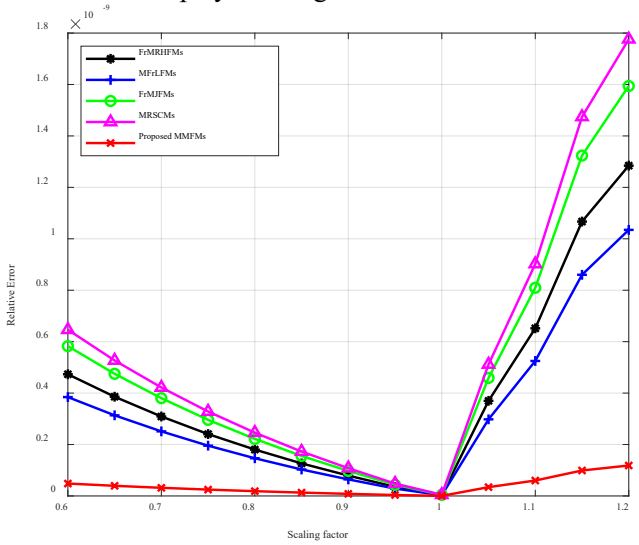

Fig.12. *RE error for the scaled images*

We find as maximum value of RE error is $1.07\,e^{-07}$ of our moments MMFMs for the three geometric transformations. Also, we notice that; the MMFMs moments take very small values for the RE error compared to tested moments.

Fig.11. *Scaled image.*

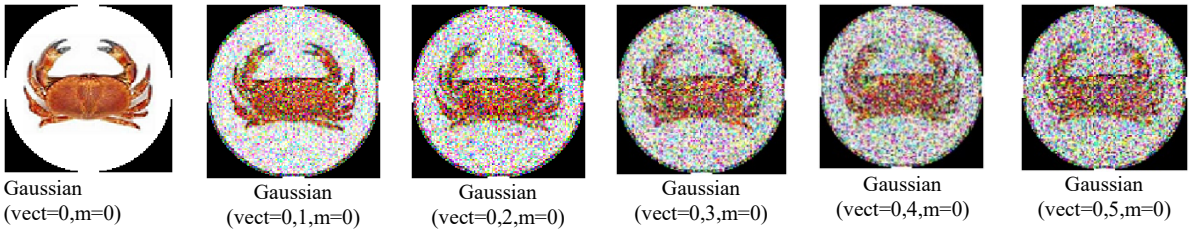

Fig.13. *Contaminated images using white Gaussian noise.*

Rigidity against noise

In this subsection, we have to study the performance of the proposed moment invariants with respect to noise invariance. Therefore, the experiment was performed to evaluate the sensitivity of different types of noise on the numerical accuracy of the proposed invariant MMFMs. In fact, the image of database 256_ObjectCategories Griffin (2007) was contaminated with different densities of Gaussian. Fig.13 shows noisy images distorted by Gaussian noise with zero mean and standard deviation varying from 0 to 0.5 with a step of 0.1. Fig.14 illustrates the robustness of MMFMs against Gaussian noise. RE error values are calculated using the proposed MMFMs and existing methods MRSCMs, FrMJFMs, MFrLFMs and FrMRHFMs.

Recognition Rates using MMFMs

In this subsection, we must use two techniques to evaluate the effectiveness of the proposed method, the first is the MMFMs-KNN architecture used K-NN (K-Nearest Neighbours with k = 1) as a classifier with the quintuple cross-validation technique, the second is the MMFMs-SVM architecture used the SVM classifier. Two databases were used; the ETHZ_53Obj database VIS @ ETH Zurich (2003) contains 270 objects classified in 70 categories where the image sizes are 320×240, and the COIL-100 database Nene *et al.* (1996) contains 7202 color images classified in 100 categories with a size unified image of 128×128 to make several experiments and tests.

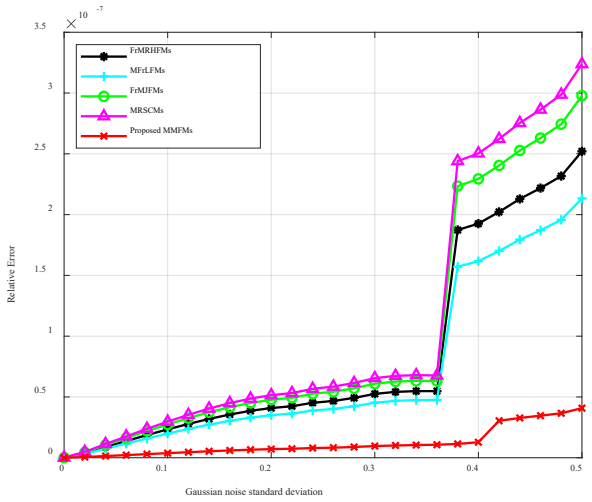

Fig.14. *RE error values of the noisy color images of 256_ObjectCategories Griffin. (2007).*

Fig.15. *The selected images from database: ETHZ_53Obj VIS @ ETH Zurich (2003)*

Table 1: *Object recognition accuracy (%) on ETHZ-53Obj database, by using existing methods.*

Moment invariants	Noise-free	Speckle noise					Average
		0.2%	0.4%	0.6%	0.8%	1%	
MMFMs-KNN	99,89	93,17	90,22	87,46	85,63	81,57	89,65
MMFMs-SVM	99,91	94,33	91,08	88,44	86,59	83,72	90,67
MRSCMs	99,70	82,80	79,03	72,37	69,17	64,18	77,87
FrMJFMs	99,45	81,01	78,24	71,58	67,38	61,39	76,50
MFrLFMs	99,87	83,93	80,16	75,45	70,3	55,31	77,50
FrMRHFMs	99,81	80,89	76,12	70,46	64,26	52,27	73,96
MZMs	98,77	75,67	70,9	65,24	62,04	54,05	71,11

Fig.16: *The selected images from database: COIL_100 Nene S. A. et al. (1996)*

We selected from the data illustrated in Figs.15 and 16 random examples of images to test our technique in a way to make several transformations, rotation, translation, scaling and mixed, in order to generate the objects from the COIL_100 Nene *et al.* (1996) database and the objects from the ETHZ_53Obj VIS @ ETH Zurich (2003) database, so we created two additional databases by adding different speckle noise densities, to see the performance of the proposed MMFMs moments about the accuracy of the classification.

Tables 1 and 2 present the comparison results in terms of object recognition accuracy for the two bases between two proposed techniques MMFMs-KNN, MMFMs-SVM and the existing methods MRSCMs, MZMs, FrMJFMs, MFrLFMs and FrMRHFMs. In addition, Fig.17 shows that our proposed models MMFMs-KNN and MMFMs-SVM provides high accuracy.

We can conclude that the results obtained for our proposed MMFMs moments are better than test moments MRSCMs, MZMs, FrMJFMs, MFrLFMs and FrMRHFMs of two databases. In terms of recognition rate, we conclude that the proposed MMFMs moments are very useful for pattern recognition and image classification.

Computation time

In this part, we must evaluate the computational efficiency of the proposed moment MMFMs compared to existing methods MRSCMs, MZMs, FrMJFMs, MFrLFMs and FrMRHFMs. Experiments are carried out to quantitatively evaluate the computation time of the proposed MMFMs. In a first step, we will evaluate the computational executions of the proposed MMFMs moments. These experiments are performed using two well-known datasets of color images, COIL_100 and ETHZ_53Obj, respectively. These datasets have different sizes and numbers of color images. A few

images are randomly selected from these datasets and displayed in Figs.15 and 16. The elapsed CPU times in seconds for the moment computation of these color images is shown in Fig.18, using the proposed method MMFMs and recent existing methods, for an increasing order of the maximum moments from 0 to 60 with a fixed increment of 10. From the results presented in Fig.18, it can be observed that the computation time taken by the proposed method is much faster than the methods existing.

Table 2: *Object recognition accuracy (%) on COIL_100 database, by using existing methods.*

Moment invariants	Noise-free	Speckle noise					Average
		0.2%	0.4%	0.6%	0.8%	1%	
MMFMs-KNN	99,83	96,13	94,12	91,60	88,13	84,27	92,34
MMFMs-SVM	99,92	97,23	95,56	93,04	91,57	88,71	94,33
MRSCMs	97,70	84,70	82,24	74,72	70,25	61,39	78,5
FrMJFMs	98,45	85,11	82,68	75,16	71,69	65,83	79,82
MFrLFMs	98,43	82,91	85,14	77,62	72,15	66,29	80,42
FrMRHFMs	97,81	86,59	84,04	79,52	76,05	70,19	82,36
MZMs	93,77	80,37	78,23	71,71	68,24	62,38	75,78

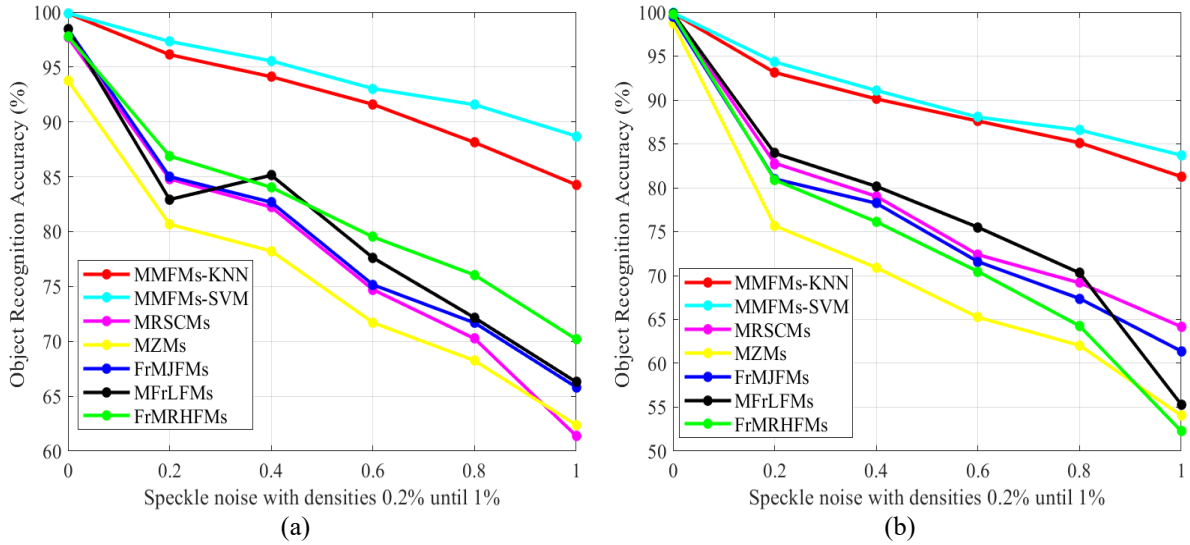

Fig.17. *Object recognition accuracy (%) using MMFMs-SVM and MMFMs-KNN: (a) dataset ETHZ_53Obj (b) dataset COIL_100.*

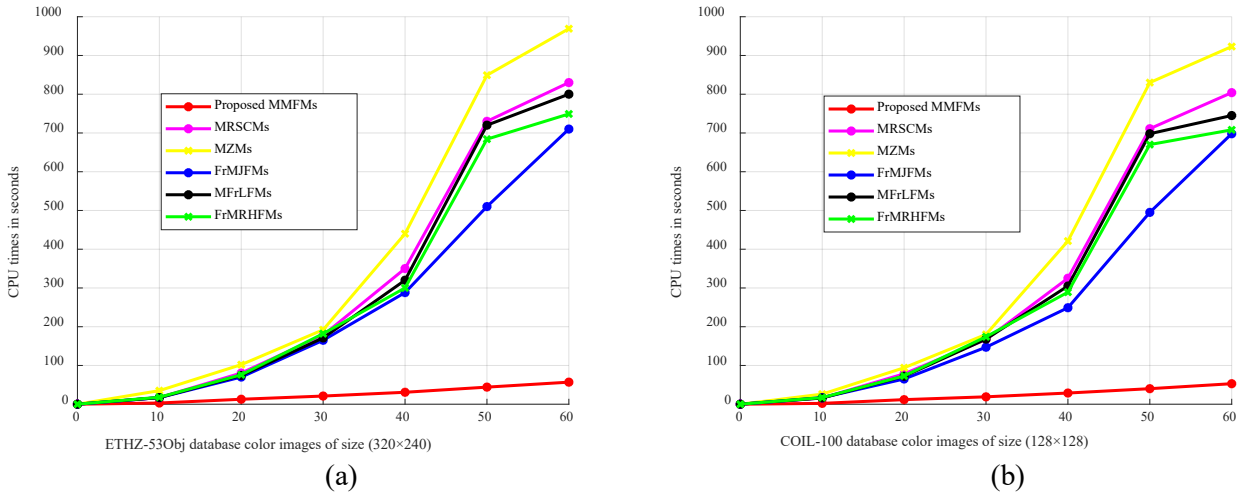

Fig.18. *The average CPU times for computing the proposed MMFMs and the existing methods :(a) dataset ETHZ_53Obj (b) dataset COIL_100.*

In the second step, we take an increasing order from 0 to 60 to generate the moment invariants and we record the elapsed CPU times, then we repeat the process 10 times to calculate the average CPU times. The results obtained clearly show that the proposed MMFMs are very fast and much faster than recent existing methods.

DISCUSSION

In the first experiment, we demonstrated the orthogonality of the Mountain functions that we used to calculate the proposed moments MMFMs. In the second experiment, we used these moments to test the reconstruction, the geometrical transformation, noise and classification of images. The results presented show the performance of MMFMs in the ability to represent and therefore correctly reconstruct color images. In fact, according to the results obtained, MMFMs produced interesting results during the recovery of color images. The information extracted by MMFMs represents multidimensional image data. In addition, the orthogonality property of the Mountain functions results in no redundancy between the values of their features, with the value of each feature representing a unique and independent character of an image. The MMFMs features provide a total view of the image because they treat the image as a whole. The effect of noise on the magnitude of the moments becomes negligible, as the moments are calculated following a summation process. Furthermore, moments are translation, rotation and scale invariant, i.e. if the query image is in a rotated or scaled version of the images in the dataset, the characteristics of the MMFMs can efficiently match and extract the most relevant images with respect to the query.

CONCLUSION

In this paper, we have proposed a new set of orthogonal moments multichannel orthogonal Mountain Fourier moments (MMFMs), based on new set of orthogonal functions called orthogonal Mountain functions for the color images. The experience shows that the images reconstructed by the orthogonal moments MMFMs are very similar to the original image when the max order approaches 63 and visualization could easily give an opinion on the degree of resemblance between the original and reconstructed images. We made comparative analysis and tests between proposed invariant moments and the test moments about invariances of geometric transformations, the results obtained show the performance of the proposed moments MMFMs on object recognition using for classification. The two sets of image data: the COIL_100 database Nene S. A. *et al.* (1996) and the ETHZ_53Obj database VIS @ ETH Zurich (2003) were used in the extensive experiments under normal image conditions and under effects of rotation, translation, scale and noise. As a general conclusion, the analysis carried out puts the proposed descriptors in favour with respect to other existing descriptors for the problems of object recognition and image classification under normal image conditions and under geometric transformations and noise conditions. According to the experimental analysis and the proposed theoretical approach, we conclude that proposed MMFMs moments are more advantageous and perform better in image recognition. The quality and the facility of the calculation of orthogonal invariant moments MMFMs show its performance in front of other orthogonal moments of test. And in future works, we will use these results to classify 3D images. We will also add parameters to our function that will allow us to detect the types of plant diseases, by the use of one of the optimization algorithms.

ACKNOWLEDGMENTS

The authors receive no funds.

The authors declare that we have no competing interests in the submission of this manuscript.

The authors would like to thank the referees for their valuable comments and suggestions.

REFERENCES

Abdulhussain SH, Mahmmod BM, AlGhadhban A, Flusser J (2022). Face recognition algorithm based on fast computation of orthogonal moments. Mathematics, 10(15): 2721. https://doi.org/10.3390/math10152721.

Abdulhussain SH, Mahmmod BM, Naser MA, Alsabah MQ, Ali R, Al-Haddad SAR (2021). A robust handwritten numeral recognition using hybrid orthogonal polynomials and moments. Sensors 21(6): 1999. https://doi.org/10.3390/s21061999.

Aboelenen T, Hosny KM, Darwish MM (2020). Novel fractional-order generic Jacobi-Fourier moments for image analysis. Signal Process 172: 107545. https://doi.org/10.1016/j.sigpro.2020.107545.

Ansary TF, Daoudi M, Vandeborre JP (2006). A bayesian 3-d search engine using adaptive views clustering. IEEE T Multimedia 9(1): 78-88. doi: 10.1109/TMM.2006.886359.

Assefa, D, Mansinha, L, Tiampo, KF, Rasmussen H, Abdella K (2010). Local quaternion Fourier transform and color image texture analysis. Signal Process 90(6): 1825-1835. https://doi.org/10.1016/j.sigpro.2009.11.031.

Bailey RR, Srinath M (1996). Orthogonal moment features for use with parametric and non-parametric classifiers. IEEE T Pattern Anal 18(4): 389-399. doi: 10.1109/34.491620.

Bao S, Song X, Hu G, Yang X, Wang C (2019). Colour face recognition using fuzzy quaternion-based discriminant analysis. Int J Mach Learn Cyb 10: 385-395. https://doi.org/10.1007/s13042-017-0722-4.

Batioua I, Benouini R, Zenkouar K (2020). Image recognition using new set of separable three-dimensional discrete orthogonal moment invariants. Multimed Tools Appl 79(19): 13217-13245. https://doi.org/ 10.1007/s11042-019-08083-1.

Batioua I, Benouini R, Zenkouar K, Zahi A (2017). 3D image analysis by separable discrete orthogonal moments based on Krawtchouk and Tchebichef polynomials. Pattern Recognition, 71: 264-277. https://doi.org/10.1016/j.patcog.2017.06.013.

Chen B, Yu M, Su Q, Shim HJ, Shi YQ (2018). Fractional quaternion Zernike moments for robust color image copy-move forgery detection. IEEE Access, 6: 56637-56646. doi: 10.1109/ ACESS. 2018.2871952.

Chen B, Yu M, Su Q, Shim HJ, Shi YQ (2018). Fractional quaternion Zernike moments for robust color image copy-move forgery detection. IEEE Access, 6: 56637-56646. doi: 10.1109/ACCESS.20 18.2871952.

Chen BJ, Shu HZ, Zhang H, Chen G, Toumoulin C, Dillenseger ZL, Luo LM (2012). Quaternion Zernike moments and their invariants for color image analysis and object recognition. Signal proces, 92(2): 308-318. https://doi.org/10.1016/j.sigpro.2011.07.018.

Chen G, Krzyzak A (2022). Feature Extraction for Patch Matching in Patch-Based Denoising Methods. Image Anal Stereol 41(3): 217-227.https://doi.org/10. 5566/ias.2812.

Darwish MM, Hosny KM, Eltoukhy MM (2020). Novel multi-channel fractional-order radial harmonic Fourier moments for color image analysis. IEEE Access, 8, 40732-40743. doi: 10.1109/ACCESS. 2020.2976759.

El Mekkaoui J, Hjouji A, Qjidaa H (2021). New set of non-separable 2D and 3D invariant moments for image representation and recognition. Multimed Tools Appl 80: 12309-12333. https://doi.org/10. 1007/s11042-020-10356-z.

El Ogri O, Daoui A, Yamni M, Karmouni H, Sayyouri M, Qjidaa H (2020). New set of fractional-order generalized Laguerre moment invariants for pattern recognition. Multimed Tools Appl 79: 23261-23294. https://doi.org/10.1007/s11042-020-09084-1.

El Ogri O, Karmouni H, Sayyouri M, Qjidaa H (2021). 3D image recognition using new set of fractional-order Legendre moments and deep neural networks. Signal Processng: Image Communication, 98, 116410. https://doi.org/10.1016/j.image.2021.116410.

Fathi IS, Ahmed MA, Makhlouf MA (2022). An efficient computation of discrete orthogonal moments for bio-signals reconstruction. EURASIP J Adv Sig Pr 2022(1): 104. https://doi.org/10.1186/s13634-022-00938-4.

Griffin G (2007). Caltech-256 Object Category Dataset. http://www.vision.caltech.edu/Image_Datasets /Caltech256/.

Guo LQ Zhu M (2011). Quaternion Fourier–Mellin moments for color images. Pattern Recognition, 44(2), 187-195.https://doi.org/10.1016/j.patcog.2010. 08.017.

He B, Liu J, Yang T, Xiao B, Peng Y (2021). Quaternion fractional-order color orthogonal moment-based image representation and recognition. EURASIP J Image Vide, 2021(1), 17. https://doi.org/10.1186 /s13 640-021-00553-7.

Hjouji A, Bouikhalene B, EL-Mekkaoui J, Qjidaa H (2021a). New set of adapted Gegenbauer–Chebyshev invariant moments for image recognition and classification. J Supercomput 77: 5637-5667. https://doi.org/10.1007/s11227-020-03450-4.

Hjouji A., Chakid R., El-Mekkaoui J. & Qjidaa H. (2021b). Adapted Jacobi orthogonal invariant moments for image representation and recognition. Circuits, Systems, and Signal Processing, 40, 2855-2882. https://doi.org/ 10.1007/s11227-022-04414-6.

Hmimid A, Sayyouri M, Qjidaa H (2015). Fast computation of separable two-dimensional discrete invariant moments for image classification. Pattern Recognition 48(2): 509-521. https://doi.org/10.1016/ j.patcog.2014.08.020.

Hosny KM, Darwish MM (2018). New set of quaternion moments for color images representation and recognition. J Math Imaging Vis 60, 717-736. https://doi.org/ 10.1007/s10851-018-0786-0.

Hosny KM, Darwish MM (2019). New set of multi-channel orthogonal moments for color image representation and recognition. Pattern Recognition 88: 153-173. https://doi.org/10.1016/j.patcog.2018.11. 014.

Hosny KM, Darwish MM, Aboelenen T (2020). New fractional-order Legendre-Fourier moments for pattern recognition applications. Pattern Recognition, 103: 107324. https://doi.org/10.1016/j.patcog.2020. 107324.

Hosny KM, Shouman, MA, Abdel Salam HM (2011). Fast computation of orthogonal Fourier–Mellin moments in polar coordinates. J Real-Time Image Pr. 6: 73-80. https://doi.org/10.1007/s11554-009-0135-z.

Hu HT, Zhang YD, Shao C, Ju Q (2014). Orthogonal moments based on exponent functions: Exponent-

Fourier moments. Pattern Recognition, 47(8): 2596-2606. https://doi.org/10.1016/ j.patcog.2014.02.014.

Hu MK (1962). Visual pattern recognition by moment invariants. IRE transactions on information theory, 8(2), 179-187. https://doi.org/10.1109/TIT. 1962.1057 692.

Idan ZN, Abdulhussain SH, Al-Haddad SAR (2020). A new separable moment based on Tchebichef-Krawtchouk polynomials. IEEE Access 8: 41013-41025. doi: 10.1109/ACCESS.2020.2977305

Janati Idrissi B, El Ogri O, EL-Mekkaoui J (2024). A new retrieval system based on quaternion radial orthogonal Jacobi moments for biomedical color images. Multimed Tools Appl: 1-25. https://doi.org/ 10.1007/s11042-023-17936-9.

Jeny AA, Junayed MS, Islam MB (2023). Deep Neural Network-Based Ensemble Model for Eye Diseases Detection and Classification. Image Anal Stereol 42(2): 77-91. https://doi.org/10.5566/ias.2857.

Ji Z, Chen Q, Sun Q, Xia DS (2009). A moment-based nonlocal-means algorithm for image denoising. Inform Process Lett 109(23-24): 1238-1244. https:// doi.org/10.1016/j.ipl. 2009.09.007.

Kanaya N, Iiguni Y, Maeda H (2002). 2-D DOA estimation method using Zernike moments. Signal processing 82(3): 521-526. https://doi.org/10.1016/ S0165-1684(01)00204-3.

Kim WY, Kim YS (2000). A region-based shape descriptor using Zernike moments. Signal Process-Image 16(1-2): 95-102. https://doi. org/ 10.1016/S0 923-5965(00)00019-9.

Lahouli I, Karakasis E, Haelterman R, Chtourou Z, De Cubber G, Gasteratos A, Attia R (2018). Hot spot method for pedestrian detection using saliency maps, discrete Chebyshev moments and support vector machine. IET Image Process 12(7): 1284-1291. https://doi.org/10.1049/iet-ipr.2017.0221.

Li FF, Andreeto M, Ranzato M, Perona P (2022). Caltech 101 (1.0) [Data set]. CaltechDATA. https://doi. org/10.22002/D1.20086.

Lin YH, Chen CH (2008). Template matching using the parametric template vector with translation, rotation and scale invariance. Pattern Recognition 41(7): 2413-2421. https://doi.org/10.1016/ j.patcog.2008.01. 017

Machhour A, Mallahi ME, Zouhri A, Chenouni D (2019). Image classification using shifted legendre-fourier moments and deep learning. In 2019 7th Mediterranean Congress of Telecommunications (CMT): pp. 1-6. IEEE. doi: 10.1109/CMT.2019.8931326.

Nene SA, Nayar SK, Murase H (1996). Columbia Object Image Library (COIL-100). Technical Report CUCS-006-96. Columbia University Department of Computer Science, New York, NY.

Ping Z, Wu R, Sheng Y (2002). Image description with Chebyshev–Fourier moments. J Opt Soc Am A 19(9): 1748-1754. ttps://doi.org/10.1364/JOSAA.19.001748.

Qi S, Zhang Y, Wang C, Zhou J, Cao X (2021). A survey of orthogonal moments for image representation: theory, implementation, and evaluation. ACM Comput Surv (CSUR) 55(1): 1-35. https://doi.org/ 10.1145/3479428.

Ren H, Ping Z, Bo W, Wu W, Sheng Y (2003). Multidistortion-invariant image recognition with radial harmonic Fourier moments. J Opt Soc Am A 20(4): 631-637. https://doi.org/10.1364/JOSAA.20. 000 631.

Sheng Y, Shen L (1994). Orthogonal Fourier–Mellin moments for invariant pattern recognition. J Opt Soc Am A: 11(6), 1748-1757. https://doi.org/10.1364/ JOSAA.11.001748.

Singh C. (2012). Local and global features-based image retrieval system using orthogonal radial moments. Opt Laser Eng 50(5): 655-667. https://doi.org/10.10 16 /j.optlaseng.2011.11.012.

Singh C, Singh J (2018). Multi-channel versus quaternion orthogonal rotation invariant moments for color image representation. Digit Signal Process 78: 376-392. https://doi.org/ 10.1016/j.dsp.2018.04.001.

Singh J, Singh C (2018). Quaternion generalized Chebyshev-Fourier and pseudo-Jacobi-Fourier moments for color object recognition. Opt Laser Technol 106: 234-250. https://doi.org/10.1016/j.opt lastec.2018.03.033.

Suk T, Flusser J (2009, September). Affine moment invariants of color images. In International Conference on Computer Analysis of Images and Patterns: pp. 334-341. Berlin, Heidelberg: Springer Berlin Heidelberg. https://doi.org/10.1007/978-3-642-03767-2_41.

Teague MR (1980). Image analysis via the general theory of moments. J Opt Soc Am 70(8): 920-930. https:// doi.org/10.1364/JOSA.70.000920.

VIS @ ETH Zurich – Visual Intelligence and Systems | ETH Zurich n.d (Created: April 2003). Datasets – Computer Vision Group | ETH Zurich.

Vite-Chávez O, Flores-Troncoso J, Olivera-Reyna R, Munoz-Minjares JU (2023). Improvement Procedure for Image Segmentation of Fruits and Vegetables Based on the Otsu Method. Image Anal Stereol 42(3): 185-196. https://doi.org/10.5566/ias.2939.

Wang C, Wang X, Li Y, Xia Z, Zhang C (2018). Quaternion polar harmonic Fourier moments for color images. Inform Sciences 450: 141-156. https://doi.org /10.1016/j.ins.2018.03.040.

Wang C, Wang X, Xia Z, Ma B, Shi YQ (2019). Image description with polar harmonic Fourier moments.

IEEE T Circ Syst Vid 30(12): 4440-4452. doi:10.1109/TCSVT.2019.2960507.

Wang XY, Li WY, Yang HY, Wang P, Li YW (2015). Quaternion polar complex exponential transform for invariant color image description. Appl Math Comput 256: 951-967. https://doi.org/10.1016/j.amc.2015.01.075.

Xiao B, Ma JF, Wang X (2010). Image analysis by Bessel–Fourier moments. Pattern Recognition 43(8), 2620-2629. https://doi.org/10.1016/j.patcog.2010.03.013.

Xiao B, Wang GY, Li WS (2014). Radial shifted Legendre moments for image analysis and invariant image recognition. Image and Vision Computing 32(12), 994-1006. https://doi.org/10.1016/j.imavis.2014.09.002.

Xin Y, Pawlak M, Liao S (2007). Accurate computation of Zernike moments in polar coordinates. IEEE T Image Process 16(2): 581-587. https://doi.org/10.1109/TIP.2006.888346.

Yamni M, Daoui A, El Ogri O, Karmouni H, Sayyouri M, Zjidaa H (2021). Accurate 2D and 3D images classification using translation and scale invariants of Meixner moments. Multimed Tools Appl 80(17): 26683-26712. https://doi.org/10.1007/s11042-020-10311-y.

Yap PT, Jiang X, Kot AC (2009). Two-dimensional polar harmonic transforms for invariant image representation. IEEE T Pattern Anal 32(7): 1259-1270. doi: 10.1109/TPAMI.2009.119.

Yu M, Chen B, Su Q, Li L (2019). Fractional quaternion cosine transforms and its application in color image copy-move forgery detection Multimed Tools Appl 78(7): 8057-8073. https://doi.org/10.1007/s11042-018-6595-z.

Zhang F, Liu SQ, Wang DB, Guan W (2009). Aircraft recognition in infrared image using wavelet moment invariants. Image Vision Computi 27(4): 313-318. https://doi.org/10 .1016/j.imavis.2008.08.007.

APPENDIX

Appendix 1

If $n = m$ then

$$\sum_{k=0}^{3+8j} e^{in\theta_{j_k}} e^{-im\theta_{j_k}} = \sum_{k=0}^{3+8j} e^{in\frac{2\pi(k+0.5)}{8j+4}} e^{-im\frac{2\pi(k+0.5)}{8j+4}} = \sum_{k=0}^{3+8j} e^{i\frac{2\pi(n-m)(k+0.5)}{8j+4}}$$
$$= \underbrace{1+1+\cdots+1}_{4+8n \text{ times}} = (4+8n).$$

Else

$$\sum_{k=0}^{3+8j} e^{in\theta_{j_k}} e^{-im\theta_{j_k}} = \sum_{k=0}^{3+8j} e^{in\frac{2\pi(k+0.5)}{8j+4}} e^{-im\frac{2\pi(k+0.5)}{8j+4}} = \sum_{k=0}^{3+8j} e^{i\frac{2\pi(n-m)(k+0.5)}{8j+4}}$$
$$= e^{i\frac{\pi(n-m)}{8j+4}} \sum_{k=0}^{3+8j} e^{i\frac{2\pi k(n-m)}{8j+4}} = e^{i\frac{\pi(n-m)}{8j+4}} \sum_{k=0}^{3+8j} e^{i\frac{2\pi k(n-m)}{8j+4}}$$
$$= e^{i\frac{\pi(n-m)}{8j+4}} \sum_{k=0}^{3+8j} \left(e^{i\frac{2\pi(n-m)}{8j+4}}\right)^k = \frac{1-\left(e^{i\frac{2\pi(n-m)}{8j+4}}\right)^{8j+4}}{1-e^{i\frac{2\pi(n-m)}{8j+4}}}$$
$$= e^{i\frac{\pi(n-m)}{8j+4}} \times \frac{1-\left(e^{i(n-m)2\pi}\right)}{1-e^{i\frac{2\pi(n-m)}{8j+4}}} \quad / \ \left(e^{i(n-m)2\pi} = 1\right)$$
$$= 0$$

Appendix 2

From Eqs.6 and 11, we can get that D_{nm} are orthogonal

$$\langle D_{nm}, D_{uv} \rangle = \sum_{j=1}^{N} \sum_{k=0}^{3+8j} D_{nm}(r_j, \alpha_{jk}) \overline{D_{uv}(r_j, \alpha_{jk})}$$

$$= \sum_{j=1}^{N} \sum_{k=0}^{3+8j} M_n(r_j) M_u(r_j) e^{i\frac{2\pi m(k+0.5)}{4+8j}} e^{-i\frac{2\pi v(k+0.5)}{4+8j}}$$

$$= \sum_{j=1}^{N} M_n(r_j) M_u(r_j) \sum_{k=0}^{3+8j} e^{i\frac{2\pi m(k+0.5)}{4+8j}} e^{-i\frac{2\pi v(k+0.5)}{4+8j}}$$

$$= \sum_{j=1}^{N} M_n(r_j) M_u(r_j) (4+8j) \delta_{mv}$$

$$= (4+8n) \delta_{nu} \delta_{mv}$$